

Electronic Supplementary Information (ESI)

Determination of Critical Concentrations by Synchronous Fluorescence Spectrometry

Daoyong Yu,^{*ab} Fang Huang^a and Hai Xu^a

^a State Key Laboratory of Heavy Oil Processing, Centre for Bioengineering and Biotechnology, China University of Petroleum, Qingdao, Shandong 266555, China

^b Laboratory of Molecular Self-assembling, Centre for Biomedical Engineering, Massachusetts Institute of Technology, Cambridge, MA 02139, USA

Note 1	The importance of determining critical concentrations.	S1
Note 2	The principle of CW-SFS determining critical concentrations. Including Figures S1-S3	S3-8
Materials	Materials	S9
Methods	Methods	S10
Table S1	Comparison between the critical concentrations determined by different methods.	S11
Figure S4	Absorption spectra and critical concentrations of Triton X-100 in MilliQ water.	S12
Figure S5	DLS analysis of Triton X-100 in MilliQ water.	S13
Figure S6	Absorption spectra and CW-SFS analysis of sodium dodecyl sulfate (SDS) in MilliQ water.	S14
Figure S7	Absorption spectra and CW-SFS analysis of Fos-Choline-14 (FC-14) in MilliQ water.	S15
Figure S8	Absorption spectra and CHCs of Chlorin e ₆ and its trisodium in ethanol.	S16
Figure S9	DLS analysis of Chlorin e ₆ in ethanol.	S17
Figure S10	DLS analysis of Chlorin e ₆ trisodium in ethanol.	S18

Note 1: The importance of determining critical concentrations.

Here critical concentration is defined as the minimum concentration of molecules at which the intermolecular hydrogen bonding, micelles, or other aggregates start forming. Thus critical concentrations include critical hydrogen-bonding concentration (CHC), critical micelle concentration (CMC), and critical aggregation concentration (CAC) etc. Critical concentrations of analytes dispersed in solvents are important parameters. It is well known, CMC is a key parameter for surfactants, and CHC and CAC are crucial parameters for biological peptides and proteins.

Hydrogen bonding is one of the main forces driving the formation of protein secondary structure, 3D net structure, micelles, and aggregates. For short peptides, their concentration has to be increased to a certain extent before the formation of intermolecular hydrogen bonding. This concentration is defined as CHC. CHC should be an important parameter for gel peptides which has not been recognized till now.

CMC is defined as the concentration of surfactants above which micelles form spontaneously. Surfactant CMC is very important in the solubilisation, isolation, stabilisation and crystallisation of membrane protein, and further for the structural analysis of membrane proteins. To isolate membrane proteins one first has to prepare the membranes, and then solubilise the membrane proteins by adding an excess of surfactant. Above CMC, surfactants form micelles by association of their hydrophobic tails, and these micelles take up lipids. Surfactants also bind to the hydrophobic surface of membrane proteins with their hydrophobic tails and possibly form a ring-like surfactant micelle surrounding the membrane protein, thus shielding the hydrophobic belt-like surface of the membrane protein from contact with water. This is the reason for surfactants to solubilise membrane proteins, although with surfactants with large polar head groups it is sometimes difficult to achieve a rapid and complete solubilisation. The solubilise, consisting of these mixed protein-surfactant complexes as well as lipid-containing and pure surfactant micelles, is then subjected to similar purification procedures as are soluble proteins. Of course, the presence of surfactants complicates the purification procedures. Therefore the surfactant screening is crucial, as the surfactant micelles have to replace and mimic the lipid bilayer as perfectly as possible, in order to maintain the stability and activity of the solubilised membrane protein. CMC is one of the necessary parameters in surfactant screening, and usually to compare the effects of different surfactants makes sense only when concentrations are above their CMCs.

For crystallisation of membrane proteins, the use of surfactant concentrations just above CMC of the respective surfactant is recommended in order to prevent complications caused by pure surfactant micelles. Suitable surfactant concentration and surfactant/protein ratio is conducive to the crystallisation of membrane proteins. Usually $5 \times \text{CMC}$ is suitable to solubilise the membrane proteins and not too much to destroy the integrity of the membrane protein, and form a better crystal. More surfactant will decrease the resolution of X-ray diffraction. On the other hand, an insufficient surfactant/protein molar ratio results in the aggregation of protein even though the surfactant concentration was above its CMC.

Unfortunately, CMC is not a constant, which can be affected by many variables. It decreases with increasing hydrophobic organic chain-length of the nonpolar groups, and for ionic surfactants it also depends on the nature and concentration of counterions in solution. Added electrolytes decrease the CMC, and the effect increases with decreasing charge density of the counterion. In biological research, it is recommended to measure the CMC in the real conditions, including buffer, temperature, and salt etc. But normally, the CMC provided by vendor had been determined in water at room temperature.

Bacterial lipopeptides are naturally occurring cyclic peptides containing a single fatty acyl chain. The structure and properties knowledge of bacterial lipopeptides has contributed to development of synthetic amphiphiles containing designed peptide sequence. Some lipopeptide surfactants had been designed for the structural study of membrane proteins¹, but no exact CMC has been reported, partly for lacking of enough sample or sensitive technique.

¹ (a) C. L. McGregor, L. Chen, N. C. Pomroy, P. Hwang, S. Go, A. Chakrabarty and G.G. Privé, *Nat. Biotechnol.*, 2003, **21**, 171; (b) G.G. Privé, *Curr. Opin. Struct. Biol.*, 2009, **19**, 379.

Peptide surfactant is a biological surfactant made from amino acids, which offers interesting alternatives to conventional surfactants in applications where renewability, biocompatibility, or added functionality may be desired. Peptide surfactant is structurally different from conventional surfactant in that its amide bond-containing backbone is distinctly different from hydrocarbon chain and offers inherently different physical properties. Designer short peptide surfactants have advantages in that they are relatively easy to design and synthesize, and some self-assembling lipid-like peptide surfactants had been used to stabilise membrane proteins². These peptides have a polar hydrophilic head and a relative nonpolar hydrophobic tail, much like other biological lipids. They use their tail to sequester the hydrophobic part of membrane proteins, and the hydrophilic heads exposed to water. Thus, they make membrane proteins soluble and stable outside of their native cellular lipid milieu. These lipid-like peptide surfactants are very important for overcoming the barrier of high resolutions of molecular structure for challenging membrane proteins³. While peptides have not been widely used in surfactant applications so far, for lack of high purity samples and exact CMCs and CACs, but recent developments may facilitate the incorporation of these interesting molecules into industrial and consumer products in the near future.

Strictly speaking, CMC is one kind of CACs. CAC is more often used in biological research for self-assembling and aggregation of membrane protein complex. For membrane protein crystallisation, it's more favorable to get fine crystals with initial concentration of dimer forming. Thus critical dimer concentration is crucial in the real buffer for membrane protein crystallisation.

² (a) X. Zhao, *Cur. Opin. Colloid Interf. Sci.*, 2009, **14**, 340; (b) P. Kiley, X. Zhao, M. Vaughn, M.A. Baldo, B.D. Bruce and S. Zhang, *PLoS Biol.*, 2005, **3**, e230. doi:10.1371/journal.pbio.0030230; (c) J.I. Yeh, S. Du, A. Tortajada, J. Paulo and S. Zhang, *Biochemistry*, 2005, **44**, 16912; (d) X. Zhao, Y. Nagai, P.J. Reeves, P. Kiley, H.G. Khorana and S. Zhang, *Proc. Natl. Acad. Sci. USA*, 2006, **103**, 17707; (e) K. Matsumoto, M. Vaughn, B.D. Bruce, S. Koutsopoulos and S. Zhang, *J. Phys. Chem. B*, 2009, **113**, 75.

³ G.G. Privé, *Curr. Opin. Struct. Biol.*, 2009, **19**, 379.

Note 2: The principle of CW-SFS determining critical concentrations.

The main analytical application of fluorescence spectrometry is the detection and quantification of species present at concentrations so low that they are inaccessible to most other techniques. The origin of fluorescence advantages can be understood in the following way. Considering the Beer-Lambert law, the fundamental relationship in quantitative absorption spectrometry is

$$A = \varepsilon bc = \lg \frac{P_0}{P_T} \quad (1)$$

where ε is the molar extinction coefficient (with dimensions of $\text{dm}^3 \cdot \text{mol}^{-1} \cdot \text{cm}^{-1}$) which is wavelength dependent, b is the optical path length (measured in centimeters) through the sample, c is the concentration (in $\text{moles} \cdot \text{dm}^{-3}$) of the analyte, P_0 is the excitation power of the incident light on the sample, and P_T is the power of the transmitted light by the sample.

The Beer-Lambert law is used to calculate the amount of absorbed excitation light by a given volume and concentration of fluorescing molecules. It is desirable to solve for the absorbed power, P_A , from Eq. (1) because the amount of fluorescence will be proportional to the absorbed power. This is given by following equation:

$$P_A = P_0 - P_T = P_0 - P_0 \cdot 10^{-\varepsilon bc} = P_0(1 - 10^{-\varepsilon bc}) \quad (2)$$

Therefore, the measured fluorescence intensity, F , is proportional to the absorbed power and the quantum yield, ϕ_F .

$$F = k \cdot \phi_F \cdot P_A = k \cdot \phi_F \cdot P_0(1 - 10^{-\varepsilon bc}) \quad (3)$$

where k is the fraction of the photons emitted by excited analyte molecules that actually are detected (often 0.10 or less). If $\varepsilon bc \rightarrow 0$, as is often the case in analytical applications of fluorometry, Eq. (3) simplifies to:

$$F = \ln 10 \cdot k \cdot \phi_F \cdot P_0 \cdot \varepsilon bc \quad (4)$$

$$\left(\lim_{x \rightarrow 0} \frac{1 - 10^{-x}}{x} = \ln 10, \text{ If } A = \varepsilon bc < 0.1, 1 - 10^{-\varepsilon bc} \approx \ln 10 \cdot \varepsilon bc, \text{ relative deviation } < 12\% \right)$$

According to Eq. (4), if the analyte concentration c is 0, the measured fluorescence signal F is 0. If c is small, F is a small number. Hence, when c is low, the measurement situation in fluorescence spectrometry, i.e. distinguishing between a small signal and zero, is more favorable than that encountered in absorption spectrometry (measuring a small difference between two large transmitted signals). The product $\varepsilon \phi_F P_0$ determines the sensitivity of fluorescence spectrometry to the analyte. In the most favorable case, the analyte absorbs strongly at the excitation wavelength, the excited analyte molecules exhibit a high probability of decaying via fluorescence, and the light source generates a large number of photons per unit time at that wavelength. If all three conditions are satisfied and the detector has high sensitivity at the wavelength at which the analyte emits, then it is possible to achieve extremely low limits of detection for the analyte, much lower than can be achieved by absorption spectrometry. This is the advantage of fluorescence.

Synchronous fluorescence spectrometry (SFS) is a method that provides information on the molecular environment in the vicinity of the fluorophores. In SFS both the excitation and emission monochromators are scanned simultaneously in such a manner that usually a constant wavelength interval ($\Delta\lambda$) is kept between emission and excitation wavelengths (CW-SFS). The spectrum is plotted as the measured fluorescence intensity against the corresponding excitation wavelength or emission wavelength. While the sensitivity of the fluorescence method is preserved, this technique offers several advantages, such as spectral simplification, bandwidth reduction, minimization of the effects of Rayleigh scattering and Raman scattering, which can both interfere in the steady-state technique. In comparison with conventional fluorescence spectroscopy, CW-SFS is preferable for the analysis of complex

multicomponent samples because it reduces spectral overlaps by narrowing spectral bands and simplifies spectra using a suitable wavelength interval.

In theory, if $\epsilon bc \rightarrow 0$, according to Eq. (4), for a given set of experimental conditions, the fluorescence intensity is linearly proportional to analyte concentration. This has been verified in fluorescence quantum yield measurement under certain experimental conditions. However, this linearity can be affected by inner-filter effects, including the excessive absorption of the excitation light (pre-filter effect) and the re-absorption of emission fluorescence (post-filter effect)⁴, which mainly lower the k value. Studies have shown that⁵, in order to minimize the inner-filter effects, absorbances in the 10 mm fluorescence cuvette should never exceed 0.1 ($A = \epsilon bc < 0.1$) at and above the excitation wavelength. Above this level, non-linear effects may be observed due to inner-filter effects, and the resulting quantum yield may be not reliable. Therefore, if the sample absorbance is less than 0.1, the fluorescence intensity should increase with analyte concentration or absorbance, and there is a good linear relationship (Figure S1), allowing accurate determination of the fluorescent quantum yield.

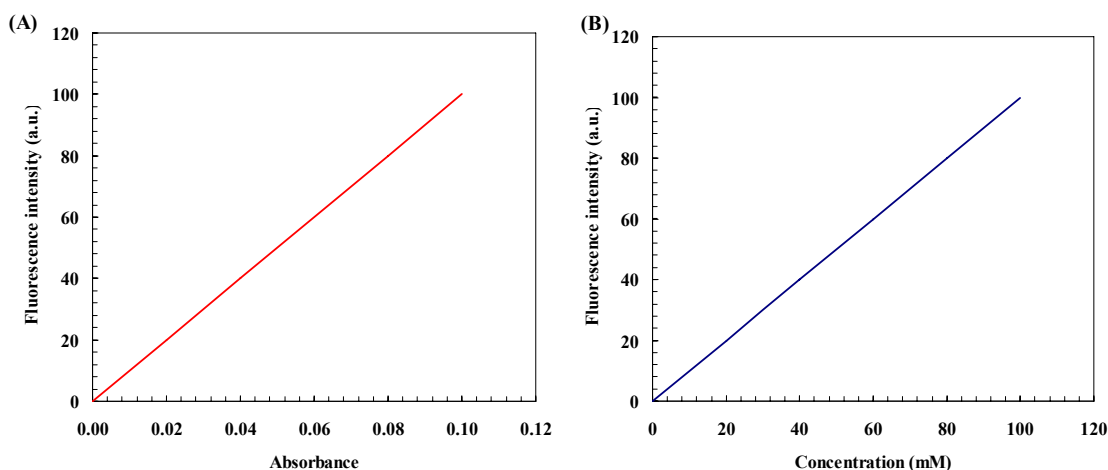


Figure S1 Linear plot of fluorescence intensity vs. absorbance and concentration.

(A) Fluorescence intensity vs. absorbance. (B) Fluorescence intensity vs. concentration of fluorescent species.

The flexible selection of an optimal λ and $\Delta\lambda$ is one of the advantages of synchronous fluorescence spectrum, which can be used to minimize inner-filter effects and achieve best linearity and sensitivity.

$$F = K \cdot c \quad (5)$$

$$K = f(k, \phi_F, P_0, \epsilon, b)$$

However, the interaction between molecules in solution and other factors will destroy this linear relationship, such as the formation of intermolecular hydrogen bonds or the formation of micelles (Figure S2), which is the principal basis for determining critical concentrations by fluorescence spectrometry or CW-SFS.

The environmental changes of a fluorophore lead to changes in fluorescence emission. Thus the synchronous fluorescence spectra of surfactants are different between in micelles and in monomers. Thus, plotting the fluorescence intensity at a particular wavelength versus surfactant concentration gives a slope change corresponding to the CMC, and the wavelength should be selected considering both fluorescence and absorption spectra in order to obtain the best selectivity and sensitivity. This novel method has been successfully applied to the CMC determination of a nonionic surfactant Triton X-100, an anionic surfactant sodium dodecyl sulphate (SDS), a lipid-like zwitterionic surfactant Fos-Choline-14 (FC-14), and some peptide surfactants (Table S1).

⁴ S. Dhama, A.J. De Mello, G. Rumbles, S.M. Bishop, D. Phillips and A. Beeby, Phthalocyanine fluorescence at high concentration: dimers or reabsorption effect? *Photochem Photobiol*, 1995, **61**(4), 341-346.

⁵ A Guide to Recording Fluorescence Quantum Yields.

<http://www.horiba.com/fileadmin/uploads/Scientific/Documents/Fluorescence/quantumyieldstrad.pdf>

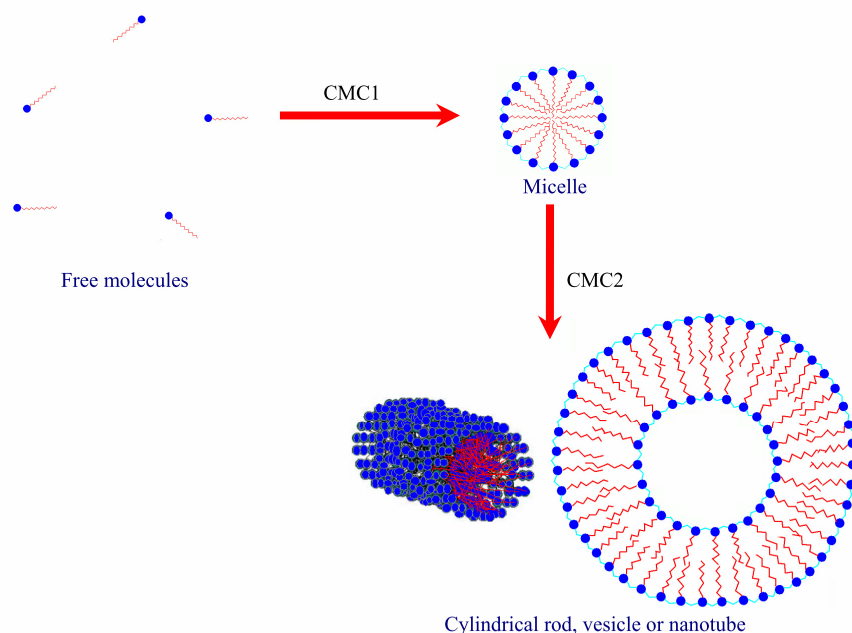


Figure S2 Schematic representation of the states in which surfactant molecules reside in solution.

CW-SFS is sensitive enough to obtain critical concentrations in very dilute solutions, but it does not necessarily show the type of aggregation by itself. However, it is often possible to use simple arguments in conjunction with the concentration data to identify possible structures. This can be illustrated with the new transition seen in Chlorin e_6 . Chlorin e_6 could in principle aggregate either through hydrogen bonding, aromatic π - π stacking, or hydrophobic interactions. In the present case, the 2 order of magnitude increase in the aggregation concentration observed of the salt of Chlorin e_6 shows that hydrogen bonding must be the key driver. Figure S3 shows a possible structure for dimer formation. Clearly, there is a very favourable conformation of the carboxylic acid groups for this dimer formation. However, once the dimer is formed further aggregation could occur through aromatic π - π stacking or hydrophobic interaction, or by some cross linking of the hydrogen bonds. At this point the CW-SFS can offer no further information. However, the sharpness of the transition does suggest that aggregation is probably more than just a dimer.

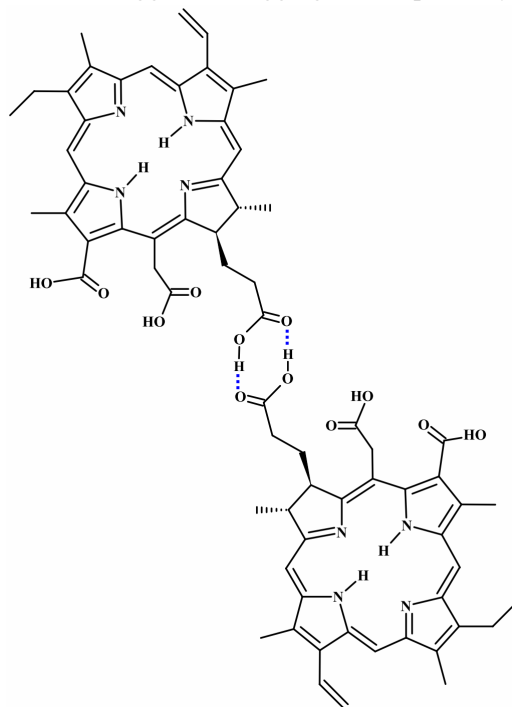
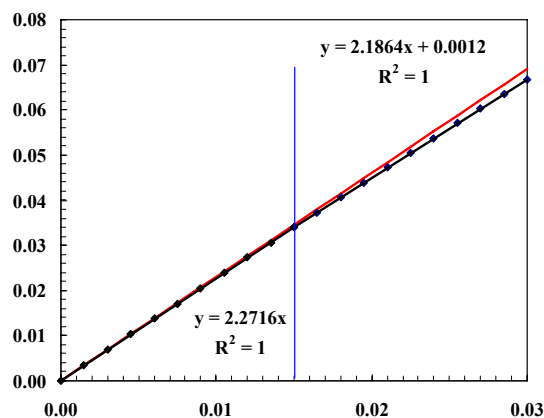
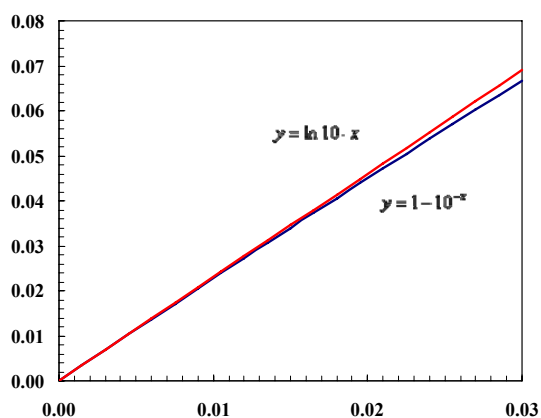
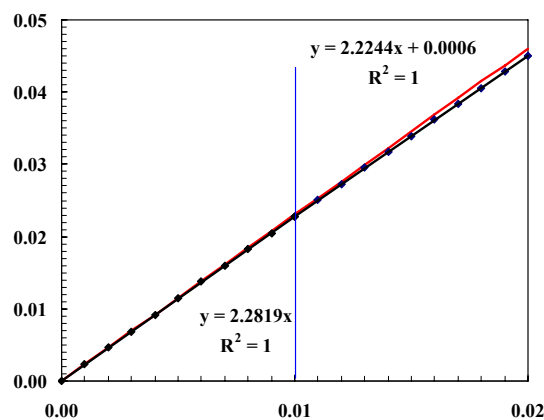
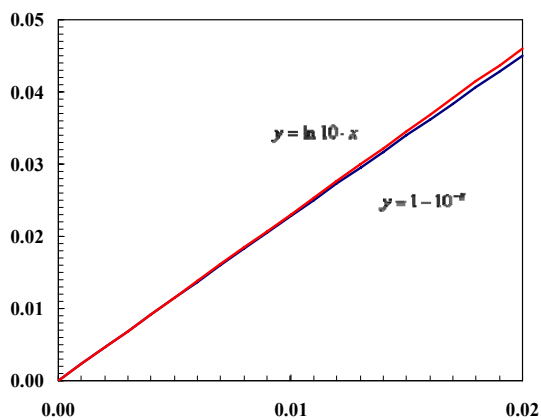
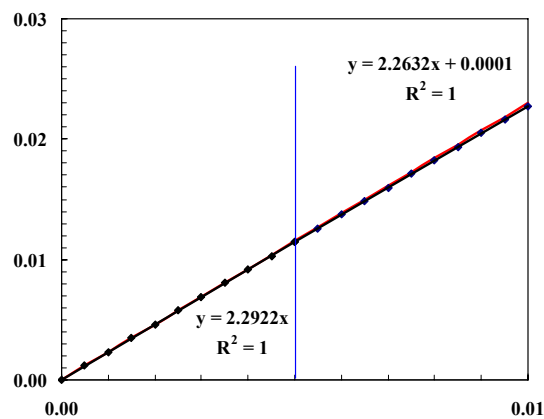
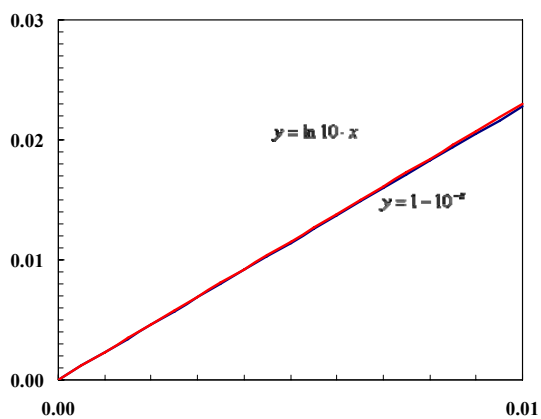


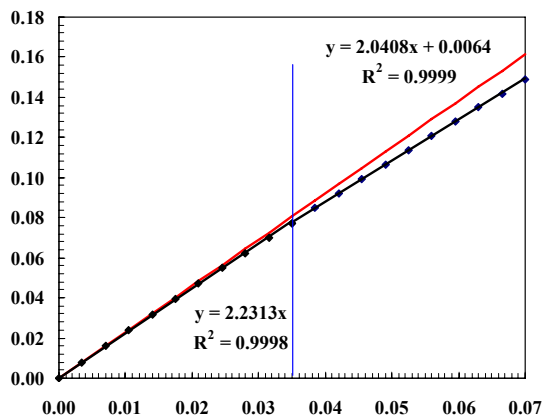
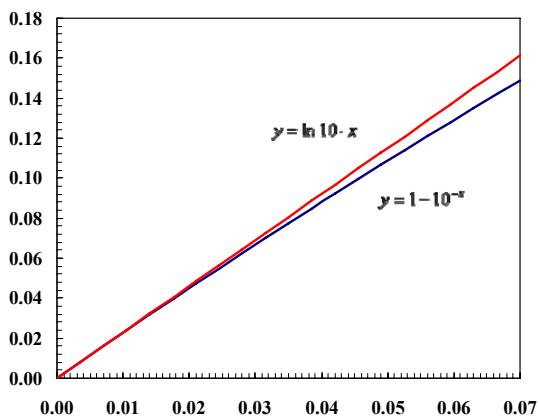
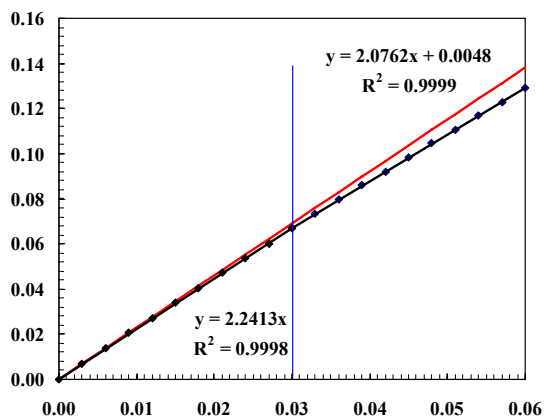
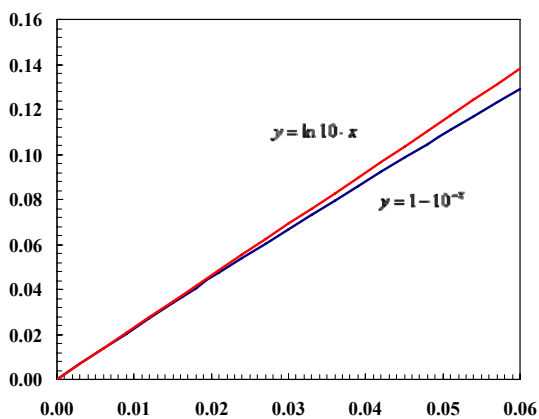
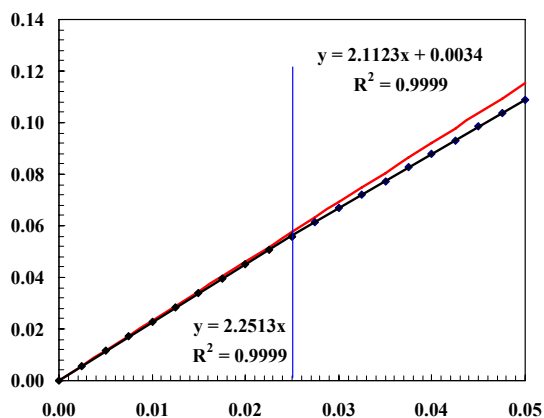
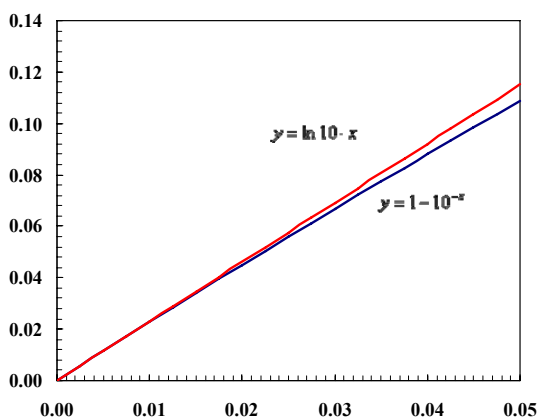
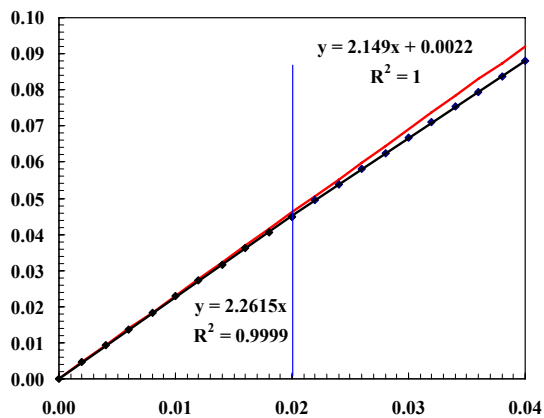
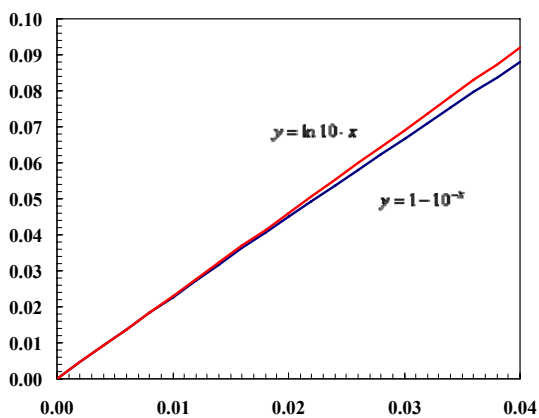
Figure S3 A possible structure for Chlorin e_6 dimer formation.

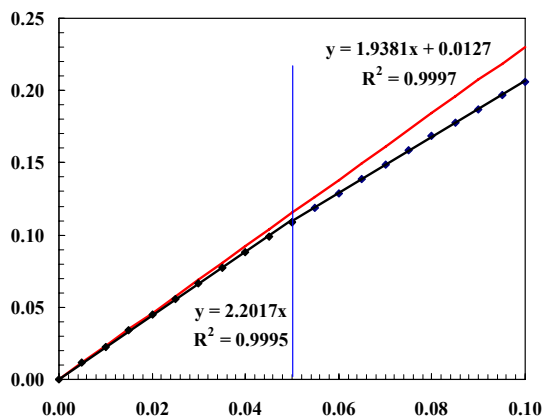
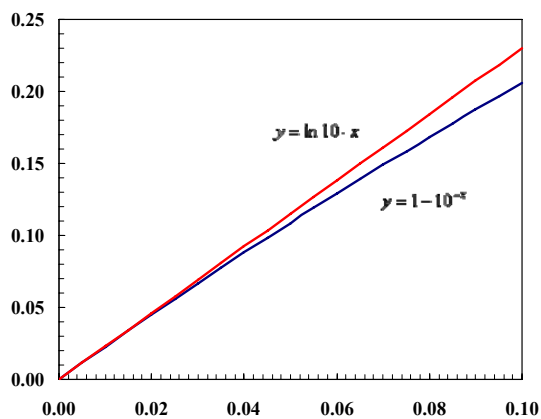
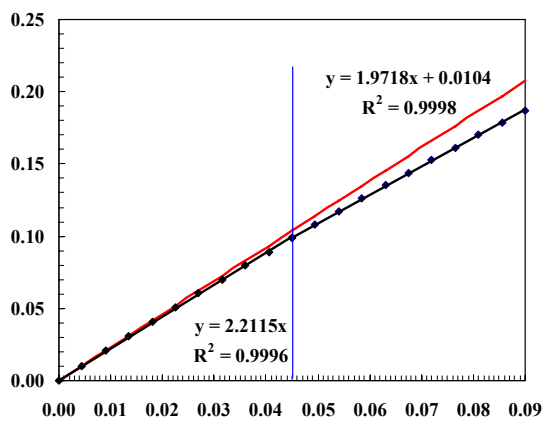
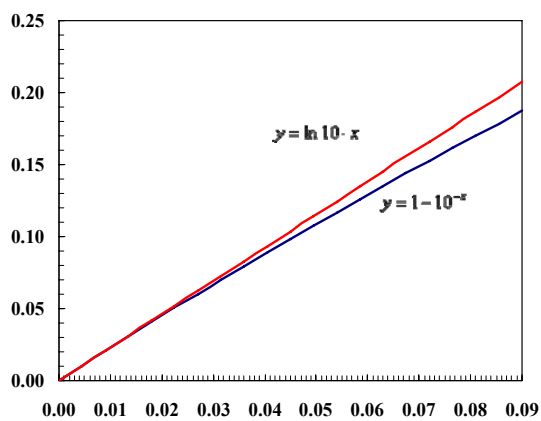
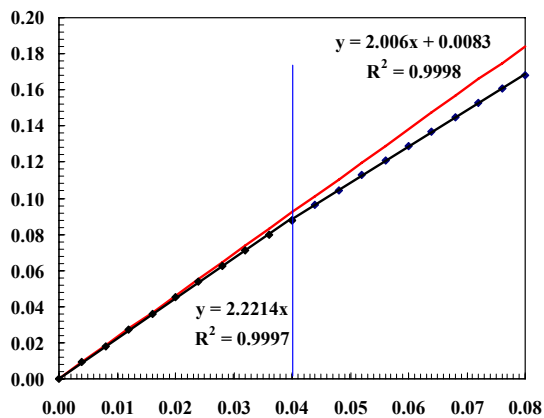
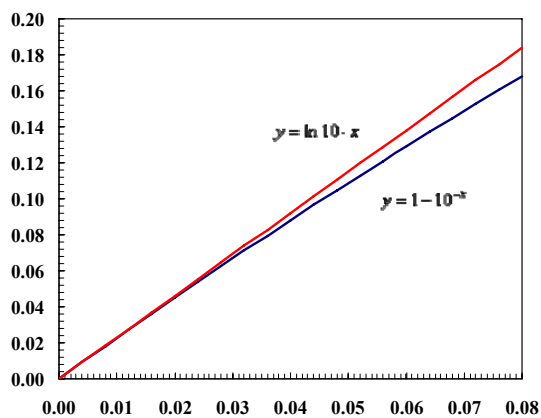
Note Appendix:

Relative deviation between Eq. (3) ($y = 1 - 10^{-x}$) and Eq. (4) ($y = \ln 10 \cdot x$), and relative changes between the two slopes for the mid-piecewise linear fittings to $y = 1 - 10^{-x}$ at different absorbance ($A = \epsilon bc$) ranges.

Absorbance range	0.01	0.02	0.03	0.04	0.05	0.06	0.07	0.08	0.09	0.10
Relative slope change, %	-1.3	-2.5	-3.8	-5.0	-6.2	-7.5	-8.5	-9.7	-10.8	-12.0



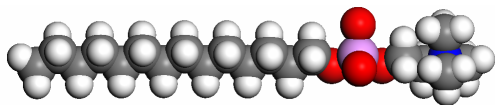




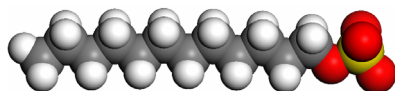
Materials

All chemicals were used originally with no further purification.

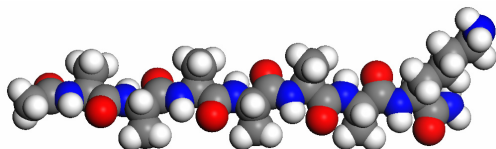
- Triton X-100 (Shelton Scientific, Inc. purity 99.0%) $C_{34}H_{62}O_{11}$, formular weight: 647(Avg)
- Chlorin e₆ trisodium salt (Tama Biochemical Co., Ltd. purity >95%) $C_{34}H_{33}N_4O_6 \cdot 3Na$, molecular weight: 662.63
- Chlorin e₆ (Frontier Scientific, Inc. purity >95%) $C_{34}H_{36}N_4O_6$, molecular weight: 596.68
- FC-14 (Fos-Choline[®]-14 sol-grade, Anatrace. purity ≥97%) $C_{19}H_{42}NO_4P$, molecular weight: 379.5



- SDS (Sodium dodecyl sulfate, Gibco BRL, Life Technologies. purity ≥99.5%) molecular weight: 288.38



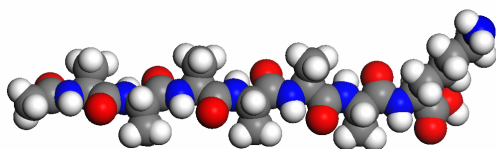
- SDBS (Sodium dodecyl benzene sulfonate, SDBS ≥90.0%, Na_2SO_4 ≤7.0%) molecular weight: 348.49
- PBS-phosphate buffer saline, Sigma. pH 7.4@25°C
(PBS: 137mM NaCl, 2.7mM KCl, 10mM Na_2HPO_4 , 1.76mM KH_2PO_4)
- Ac-A₆K-CONH₂ (CPC Scientific, Inc. purity >80%) molecular weight 613.7; iso-electric point, pI=14. Length is about 3.0nm.



Dissolved in MilliQ water, pH=3.2, positive charged.

Neutralized with 1M NaOH, pH=7.0, positive charged.

- Ac-A₆K-COOH (CPC Scientific, Inc. purity >80%) molecular weight 614.7; iso-electric point, pI 6.4. Length is about 3.0nm.



Dissolved in MilliQ water, pH=3.5, negative charged.

Neutralized with 1M NaOH, pH=6.7, a little negative charged.

The impurities in Ac-A₆K-CONH₂ and Ac-A₆K-COOH are mostly peptides with modified sequences, except for trifluoroacetic acid (TFA) salt.

Methods

Ultraviolet-visible spectrometry

Absorption spectra of samples were taken using Cary 6000i UV-Vis-NIR spectrophotometer with data intervals of 1 nm and spectral regions between 200 and 800 nm. All the measurements were made at room temperature 23°C. The absorption spectra of samples were corrected with solvent spectra. Quartz sample cells with optical paths of 10 mm were used (NSG Precision Cells, type 23 UV). The critical concentration was determined from a plot of the absorbance at a fixed wavelength versus the sample concentration.

Constant wavelength synchronous fluorescence spectrometry (CW-SFS)

We performed CW-SFS measurements using the SPEX FluoroMax-2 with a 4-position sample changer, and the emission light was collected at 90°. The energy emitted by samples was recorded while varying the excitation and emission wavelengths simultaneously. The difference $\Delta\lambda$ was kept constant at 20 nm. The fluorescence intensity data was corrected for the changes in excitation intensity by dividing the spectrally corrected emission data by the spectrally corrected excitation intensity, corresponding to S_c/R_c . Note that all the fluorescence spectra must be recorded with constant slit widths. Changing this parameter between samples will invalidate the measurement. Ideally the band pass of the excitation monochromator should be set to the same value as the UV-vis absorbance spectrometer used for the absorbance measurements⁶.

$\Delta\lambda \geq 20$ nm is commonly recommended to avoid the interference of excitation light with emission intensity. $\Delta\lambda$ should first be optimized for maximum sensitivity, and this can be done by measuring the excitation and emission spectra and determining the difference between the excitation and the emission maxima.

Dynamic light scattering (DLS)

We performed DLS experiments on the Precision Detectors Model PDDL/BS (Precision Detectors, Franklin, MA) with an 800 nm laser operating at 100 mW. The scattered light was collected at a 90° angle. Data were acquired and analyzed by Precision Deconvolve program. For a typical DLS experiment, 200 μ L of a sample solution was slowly pipetted into a clean quartz micro-cuvette.

In DLS (http://www.ap-lab.com/light_scattering.htm) one measures the time dependence of the light scattered from a very small region of solution, over a time range from tenths of a microsecond to milliseconds. These fluctuations in the intensity of the scattered light are related to the rate of diffusion of molecules in and out of the region being studied (Brownian motion), and the data can be analyzed to directly give the diffusion coefficients of the particles doing the scattering. When multiple species are present, a distribution of diffusion coefficients is seen. Traditionally, rather than presenting the data in terms of diffusion coefficients, the data are processed to give the size of the particles (radius or diameter). The relation between diffusion and particle size is based on theoretical relationships for the Brownian motion of spherical particles. The hydrodynamic diameter or Stokes radius, R_h , derived from this method is the size of a spherical particle, and the data is commonly presented as the fraction of particles as a function of their diameter.

Surface tension measurement / Tensiometry

The surface tension experiments were performed by Wilhelmy plate method using a K20 Krüss tensiometer at a controlled room temperature (23±1°C). The accuracy of the measurement was within ±0.1 mN/m. Before the measurement, the platinum plate was cleaned with a dilute solution of chromic acid mixture and washed thoroughly with pure water and then heated to redness using the oxidizing portion of the flame of a Bunsen burner. The various concentrations of Triton X-100 solutions were prepared by addition of small aliquots of concentrated Triton X-100 solution to 25 ml of sample.

Conductometry

The specific conductivity (μ S/cm) measurements of samples were measured in a thermostatic glass cell using a DDS-307 digital conductometer from Shanghai Precision & Scientific Instrument. Bright Pt and black Pt conductivity electrodes were used respectively for low concentration and high concentration samples.

⁶ A Guide to Recording Fluorescence Quantum Yields.

<http://www.horiba.com/fileadmin/uploads/Scientific/Documents/Fluorescence/quantumyieldstrad.pdf>

Table S1

Table S1. Comparison between the critical concentrations determined by different methods

Analyte	Solvent	Testing technique [†]	Critical concentrations [‡] (mM)			
			CHC	CMC1	CMC2	
Chlorin e ₆	Ethanol	CW-SFS	$(4.41 \pm 0.05) \times 10^{-4}$	n.a.	n.a.	
		AS	$(4.41 \pm 0.05) \times 10^{-4}$	n.a.	n.a.	
Chlorin e ₆ 3Na	Ethanol	CW-SFS	0.075 ± 0.005	n.a.	n.a.	
		AS	0.075 ± 0.005	n.a.	n.a.	
Triton X-100	MilliQ water	ST	n.a.	0.19 ± 0.05	n.a.	
		CW-SFS	0.016 ± 0.005	0.19 ± 0.05	1.25 ± 0.05	
		AS	n.a.	0.22 ± 0.05	1.29 ± 0.05	
SDS	MilliQ water	ST	n.a.	6.94 ± 0.10	n.a.	
		CW-SFS	n.a.	6.65 ± 0.10	40.4 ± 0.5	
		EC	n.a.	7.95 ± 0.10	43.7 ± 0.5	
FC-14	MilliQ water	SFS	n.a.	0.14 ± 0.05 (0.12^7)	0.76 ± 0.05	
SDBS ⁸	MilliQ water	ST	n.a.	1.40 ± 0.05	n.a.	
		CW-SFS	n.a.	1.48 ± 0.05	6.90 ± 0.05	
		AS	n.a.	1.58 ± 0.05	7.36 ± 0.05	
		EC	n.a.	1.63 ± 0.05	7.72 ± 0.05	
Ac-A ₆ K-CONH ₂	MilliQ water (pH 3.5±0.5)	ST	n.a.	0.49 ± 0.05	n.a.	
		CW-SFS	0.081 ± 0.005	0.49 ± 0.05	n.d.	
		AS	n.d.	0.65 ± 0.05	2.44 ± 0.05	
		EC	n.d.	0.65 ± 0.05	2.44 ± 0.05	
	MilliQ water pH 7.0 ⁹	CW-SFS	0.016 ± 0.005	0.20 ± 0.05	1.00 ± 0.05	
		AS	n.d.	0.20 ± 0.05	1.00 ± 0.05	
		PBS (pH 7.4)	ST	n.a.	0.025 ± 0.005	n.a.
			CW-SFS	n.d.	0.028 ± 0.005	0.10 ± 0.05
AS	n.d.	0.029 ± 0.005	0.11 ± 0.05			
	Ac-A ₆ K-COOH	MilliQ water (pH 3.5±0.5)	ST	n.a.	0.41 ± 0.05	n.a.
CW-SFS			0.032 ± 0.005	0.41 ± 0.05	2.28 ± 0.05	
AS			n.d.	0.49 ± 0.05	2.28 ± 0.05	
EC			n.d.	0.52 ± 0.05	2.36 ± 0.05	
MilliQ water pH 6.7 ¹⁰		CW-SFS	n.d.	0.081 ± 0.005	0.49 ± 0.05	
		AS	n.d.	0.081 ± 0.005	0.57 ± 0.05	
		PBS (pH 7.4)	CW-SFS	0.0032 ± 0.0005	0.041 ± 0.005	0.20 ± 0.05
AS	n.d.		0.049 ± 0.005	0.20 ± 0.05		

[†] ST: Surface tension; CW-SFS: Constant wavelength synchronous fluorescence spectrometry; AS: Molecular absorption spectrometry; EC: Electrical conductivity.

* n.a.: not available; n.d.: not determined.

[‡] CHC: Critical hydrogen-bonding concentration; CMC1: Critical micelle concentration 1; CMC2: Critical micelle concentration 2.

⁷ From product data sheet.

⁸ J. Zhang, Y. Qiu, D-Y. Yu, Critical micelle concentration determination of sodium dodecyl benzene sulfonate by synchronous fluorescence spectrometry. *Chinese Journal of Applied Chemistry*, 2009, **26**(12), 1480-1483.

⁹ 1 M NaOH neutralized.

¹⁰ 1 M NaOH neutralized.

Figure S4 Absorption spectra and critical concentrations of Triton X-100 in MilliQ water.

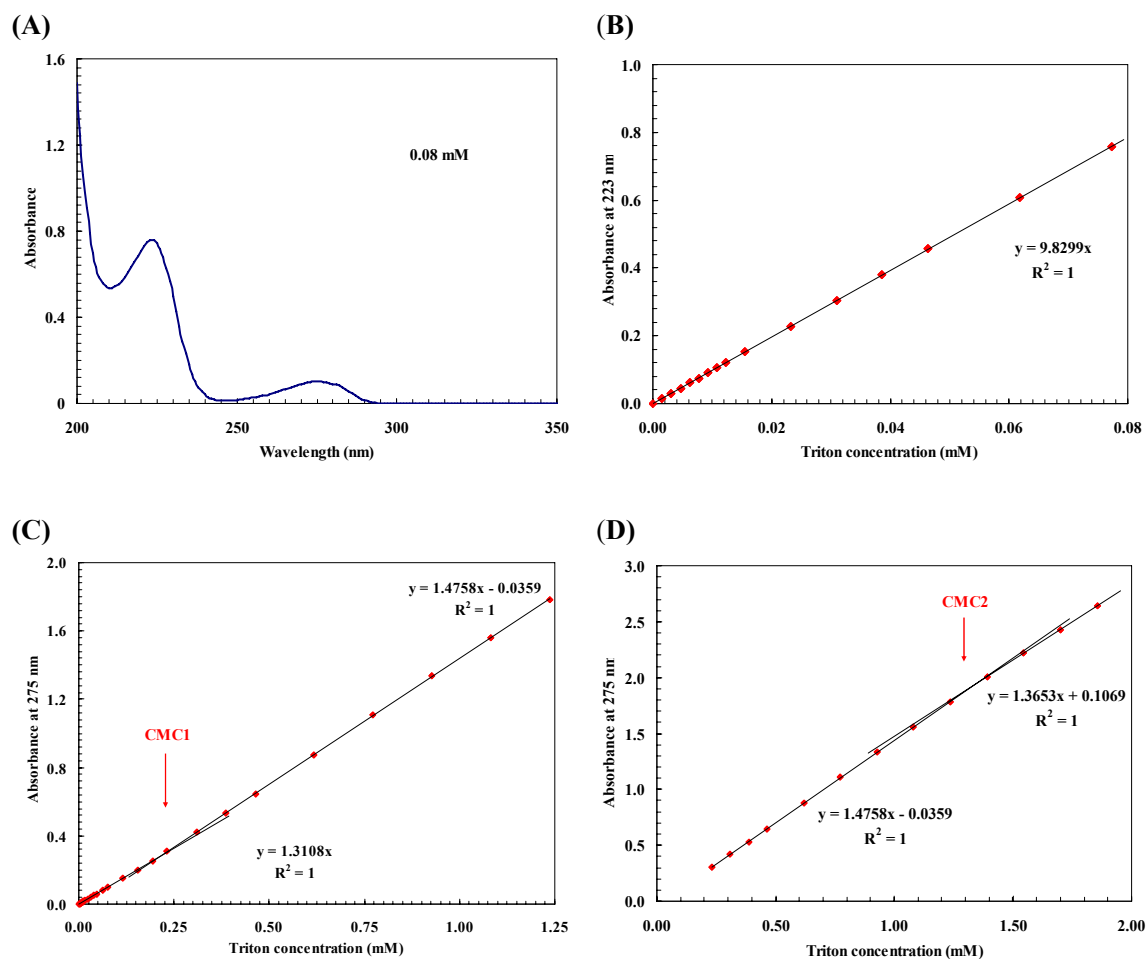


Figure S4 Absorption spectra and critical concentrations of Triton X-100 in MilliQ water. (A) Absorption spectra of Triton X-100 in MilliQ water. (B) Plot of absorbance at 223 nm versus dilute Triton X-100 concentration, without apparent slope change. (C) Plot of absorbance at 275 nm versus Triton X-100 concentration with slight slope change. (D) Plot of absorbance at 275 nm versus Triton X-100 concentration with slight slope change. (B,C,D) mean of 5 runs and the error bars are less than the data symbols.

Figure S5 Dynamic light scattering (DLS) analysis of Triton X-100 in MilliQ water.

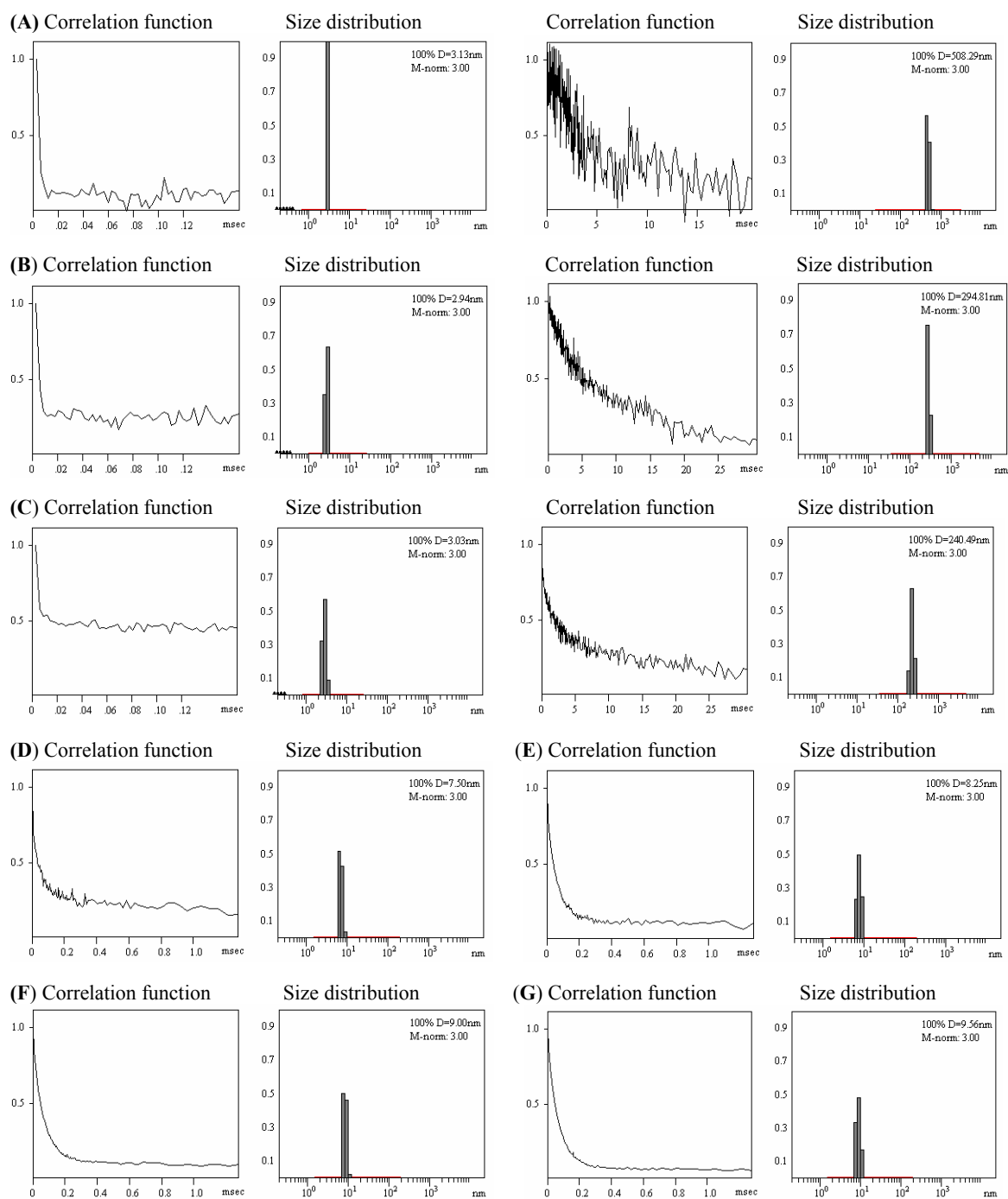


Figure S5 DLS analysis of Triton X-100 in MilliQ water. The correlation function derived from the data and the size distribution computed by PrecisionDeconvolve is displayed. **(A)** Triton X-100 in MilliQ water **0.008 mM**. Over a time range tenth of a millisecond, the correlation function baseline is around zero, and Triton X-100 monomers with apparent diameter about 3 nm were detected. Meanwhile over a long time range tens of milliseconds, few larger assembling particles with diameter around 500 nm were detected. **(B)** Triton X-100 in MilliQ water **0.08 mM**. Over a time range tenth of a millisecond, the correlation function baseline is far from zero, and Triton X-100 monomers with apparent diameter about 3 nm were detected. Meanwhile over a long time range tens of milliseconds, larger assembling particles with diameter around 300 nm were detected. **(C)** Triton X-100 in MilliQ water **0.15 mM**. Over a time range tenth of a millisecond, the correlation function baseline is around zero, and Triton X-100 monomers with apparent diameter about 3 nm were detected. Meanwhile over a long time range tens of milliseconds, larger assembling particles with diameter around 240 nm were detected. **(D)** Triton X-100 in MilliQ water **0.8 mM**. The correlation function baseline is around zero, and Triton X-100 micelles with apparent diameter about 7.5 nm were detected. **(E)** Triton X-100 in MilliQ water **1.5 mM**. The correlation function baseline is around zero, and micelles bumped into each other and formed larger aggregates with apparent diameter about 8.2 nm. **(F)** Triton X-100 in MilliQ water **3.0 mM**. The correlation function baseline is around zero, and micelles bumped into each other and formed larger aggregates with apparent diameter about 9.0 nm. **(G)** Triton X-100 in MilliQ water **4.5 mM**. The correlation function baseline is around zero, and micelles bumped into each other and formed larger aggregates with apparent diameter about 9.5 nm.

Figure S6 Absorption spectra and CW-SFS analysis of sodium dodecyl sulfate (SDS) in MilliQ water.

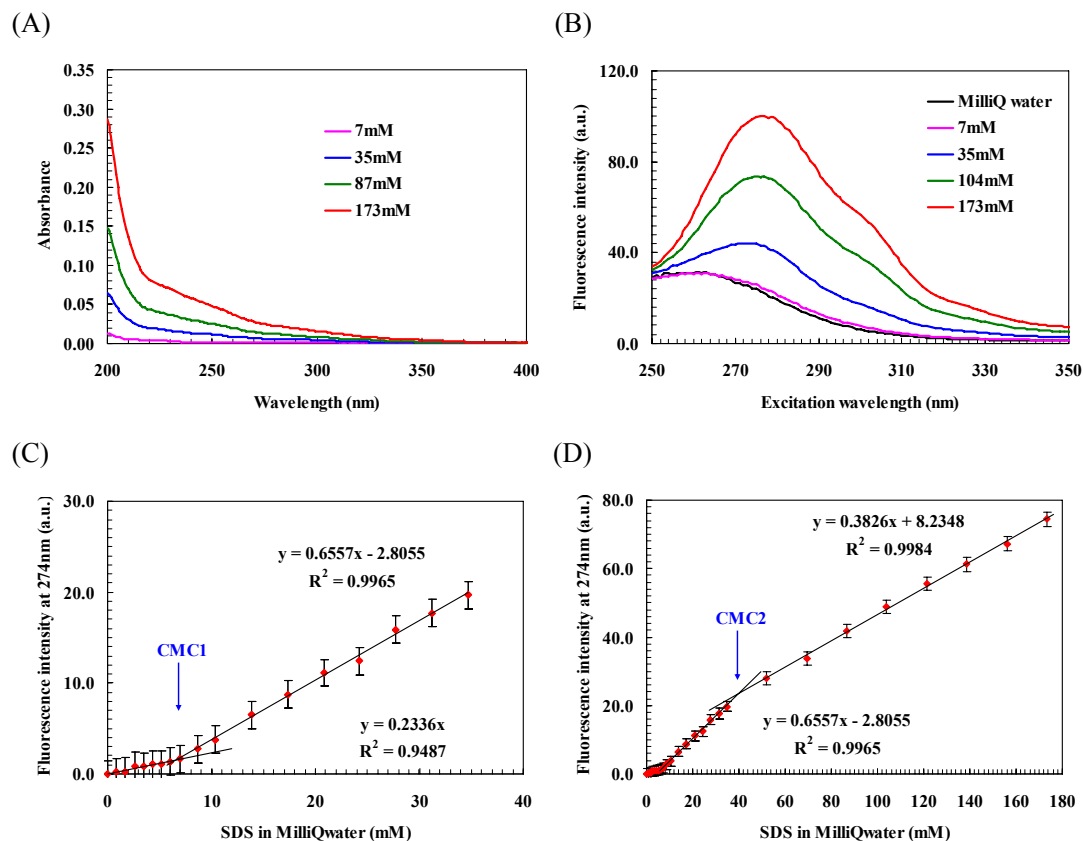


Figure S6 CW-SFS analysis of sodium dodecyl sulfate (SDS) in MilliQ water. (A) Absorption spectra of SDS in MilliQ water. (B) SFS spectra of SDS in MilliQ water. (C) CMC1, the relative slope change is 180.7%. (D) CMC2, the relative slope change is -41.7% which is much greater than the theoretical slope change -6.2% with $A_{\geq 274\text{nm}} < 0.05$. (C,D) mean of 5 runs.

Figure S7 Absorption spectra and CW-SFS analysis of Fos-Choline-14 (FC-14) in MilliQ water.

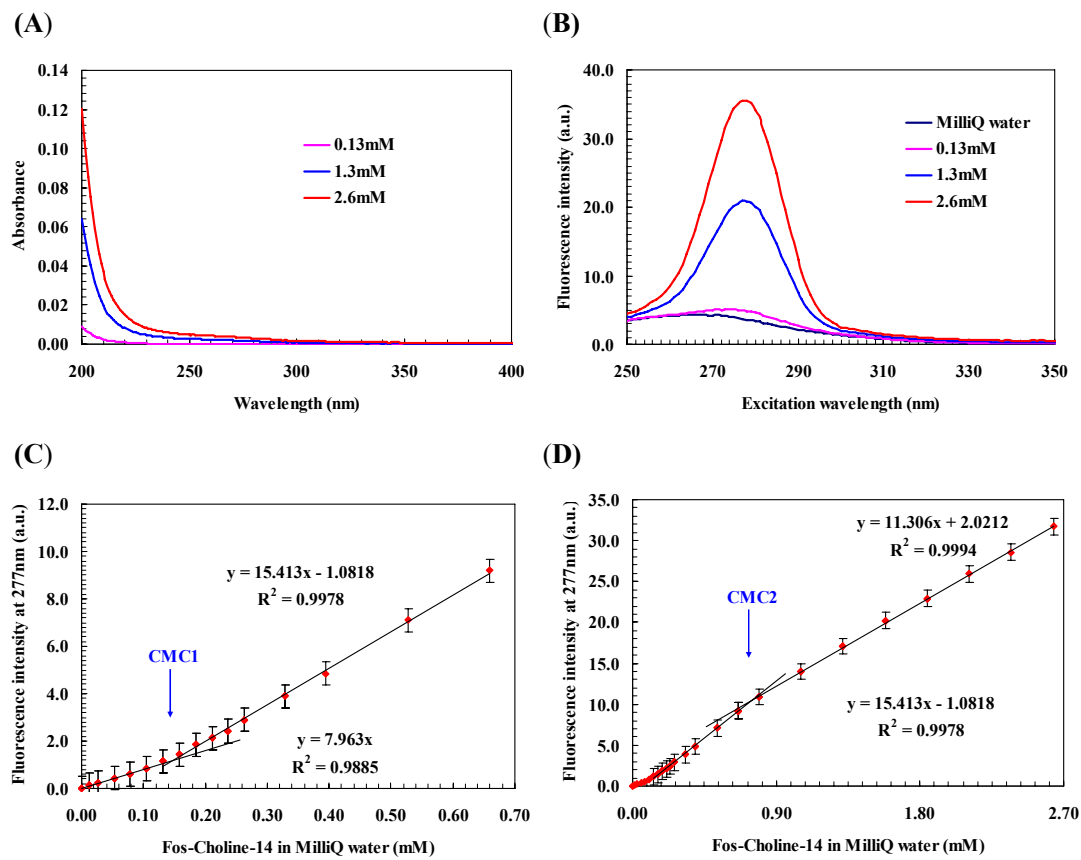


Figure S7 CW-SFS analysis of Fos-Choline-14 (FC-14) in MilliQ water. (A) Absorption spectra of FC-14 in MilliQ water. (B) SFS spectra of FC-14 in MilliQ water. (C) CMC1, the relative slope change is 97.6%. (D) CMC2, the relative slope change is -26.6% which is much greater than the theoretical slope change -1.3% with $A_{\geq 277\text{nm}} < 0.01$. (C,D) mean of 5 runs.

Figure S8 Absorption spectra and CHCs of Chlorin e_6 and its trisodium in ethanol.

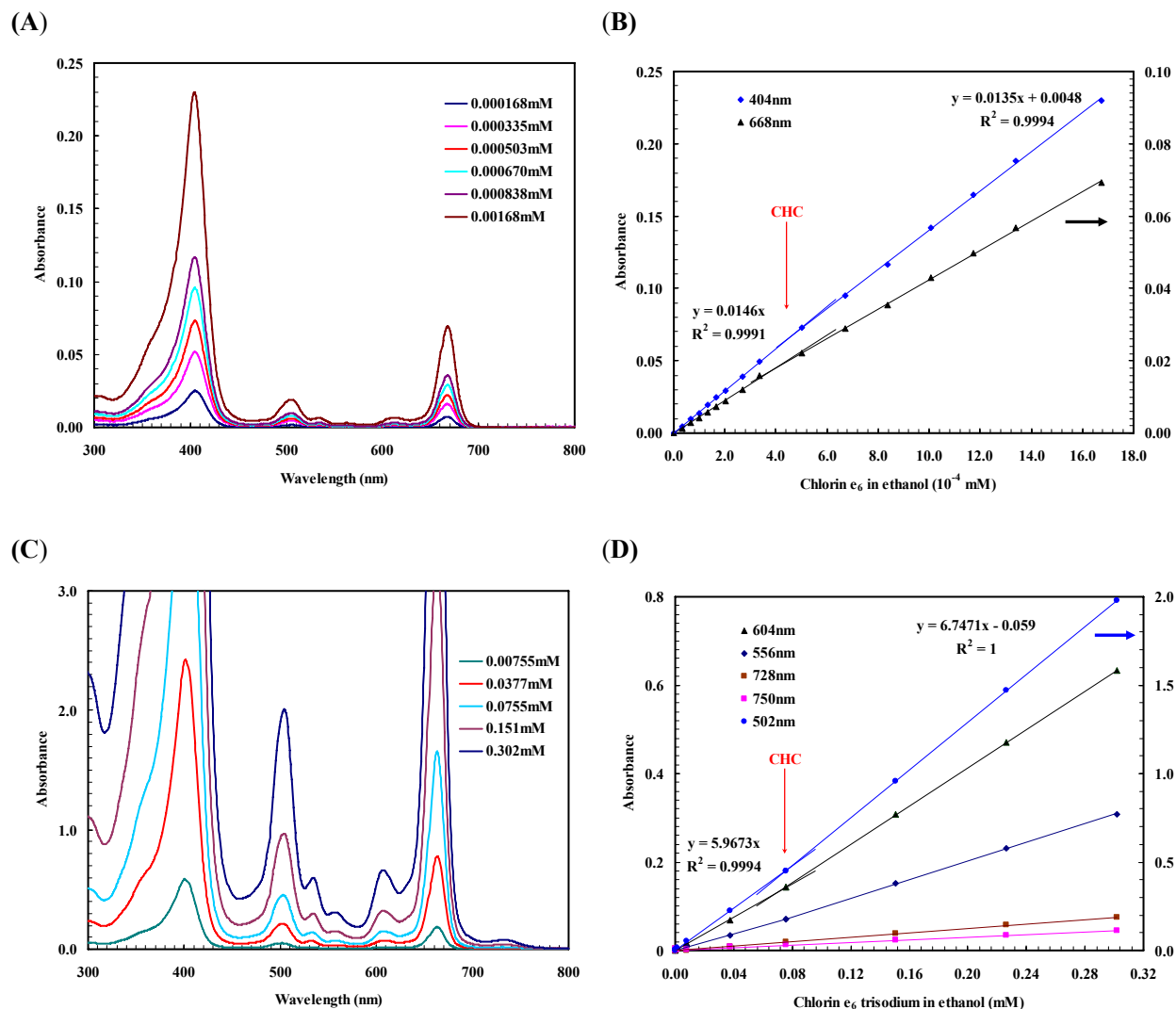


Figure S8 Absorption spectra and CHCs of Chlorin e_6 and its trisodium in ethanol. (A) Absorption spectra of Chlorin e_6 in ethanol. (B) Plot of absorbance versus Chlorin e_6 concentration with slight slope change. (C) Absorption spectra of Chlorin e_6 trisodium in ethanol. (D) Plot of absorbance versus Chlorin e_6 trisodium concentration with slight slope change. (B,D) mean of 5 runs and the error bars are less than the data symbols.

Figure S9 DLS analysis of Chlorin e_6 in ethanol.

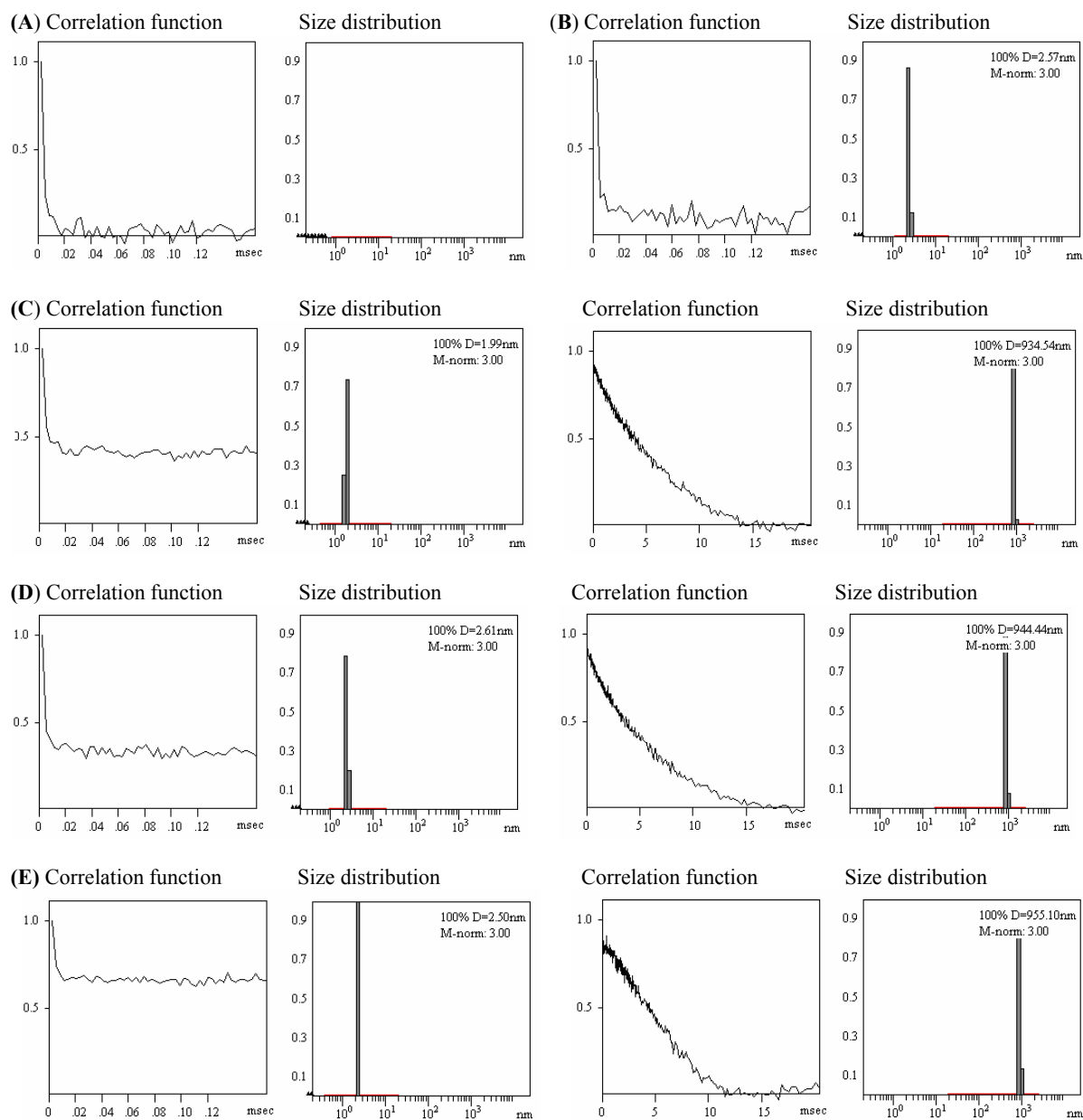


Figure S9 DLS analysis of Chlorin e_6 in ethanol. The correlation function derived from the data and the size distribution computed by PrecisionDeconvolve is displayed. **(A)** Pure ethanol. Over a time range tenth of a millisecond, the correlation function baseline is zero, and no 1-20 nm particle was detected. **(B)** Chlorin e_6 in ethanol, $6.70 \times 10^{-5} \text{ mM} < \text{CHC}$. Over a time range tenth of a millisecond, the correlation function baseline is about zero, and Chlorin e_6 monomers with apparent diameter about 2-3 nm were detected. **(C)** Chlorin e_6 in ethanol, $6.70 \times 10^{-3} \text{ mM} > \text{CHC}$. Over a time range tenth of a millisecond, the correlation function baseline is far from zero, and Chlorin e_6 monomers with apparent diameter about 2-3 nm were detected. Meanwhile over a long time range tens of milliseconds, larger assembling particles with diameter around 900 nm were detected. **(D)** Chlorin e_6 in ethanol, $3.35 \times 10^{-2} \text{ mM} > \text{CHC}$. Over a time range tenth of a millisecond, the correlation function baseline is far from zero, and Chlorin e_6 monomers with apparent diameter about 2-3 nm were detected. Meanwhile over a long time range tens of milliseconds, larger assembling particles with diameter around 900 nm were detected. **(E)** Chlorin e_6 in ethanol, $1.68 \times 10^{-1} \text{ mM} > \text{CHC}$. Over a time range tenth of a millisecond, the correlation function baseline is far from zero, and Chlorin e_6 monomers with apparent diameter about 2-3 nm were detected. Meanwhile over a long time range tens of milliseconds, larger assembling particles with diameter around 900 nm were detected.

